

Reinforcement Learning Enhancing Entanglement for Two-Photon-Driven Rabi Model

Tingting Li ^{†,1} Yiming Zhao ^{†,1} Yong Wang,¹ Yanping Liu,¹ Yazhuang Miao,¹ and Xiaolong Zhao^{*1}

¹*School of Science, Qingdao University of Technology, Shandong, China*

(Dated: December 2, 2024)

A control scheme is proposed that leverages reinforcement learning to enhance entanglement by modulating the two-photon-driven amplitude in a Rabi model. The quantum phase diagram versus the amplitude of the two-photon process and the coupling between the cavity field and the atom in the Rabi model, is indicated by the energy spectrum of the hybrid system, the witness of entanglement, second order correlation, and negativity of Wigner function. From a dynamical perspective, the behavior of entanglement can reflect the phase transition and the reinforcement learning agent is employed to produce temporal sequences of control pulses to enhance the entanglement in the presence of dissipation. The entanglement can be enhanced in different parameter regimes and the control scheme exhibits robustness against dissipation. The replaceability of the controlled system and the reinforcement learning module demonstrates the generalization of this scheme. This research paves the way of positively enhancing quantum resources in non-equilibrium systems.

I. INTRODUCTION

The interaction between a two-level system and an electromagnetic field, fully described by the quantum Rabi model [1, 2] is a platform which has widespread utility ranging from the study of fundamental physics [3] to the cutting edge of quantum information [4]. In the regime of cavity quantum electrodynamics (QED), when the cavity-qubit coupling rate is strong enough to dominate dissipation rates or reaches the domain of transition frequencies of the cavity or qubit, the counter-rotating term cannot be ignored, and the system is best described by the quantum Rabi model [4, 5]. Once the coupling is strong enough, a wide range of interesting phenomena occurs, including innovative quantum phase transitions in the single-qubit-single-oscillator model when the frequency of the oscillator is much lower than that of the qubit [6, 7], generation of pure-cat-state [8, 9], strongly entangled states, and novel steady-state squeezing [10]. To date, in specially designed architectures, the qubit-cavity coupling rate can reach the considerable fraction of the cavity transition frequency [11]. By inductively coupling a flux qubit and an LC oscillator via Josephson junctions, ultrastrong-coupling regime with unconventional transition spectra has been realized [12]. Quantum simulation in circuit QED provides an experimental access to the physics of the ultrastrong-and deep-strong coupling regimes of an effective quantum Rabi model [13, 14]. The strong coupling limit of cavity QED has been demonstrated in a solid-state system by the vacuum Rabi mode splitting and the corresponding avoided crossings [15].

The periodically kicked pulsed pump field of a cavity in the presence of Kerr medium acts as a parametric amplifier to investigate nonclassical behaviors of the mean photon number [16]. In a cavity QED setup, the time-dependent two-photon parametric driving can enhance the light-matter coupling and generate entanglement [17, 18]. Nonclassical cavity mode can be generated through a nonlinear optical parametric amplifier

with amplitude determined by pump field [19]. Robust photonic cat states can be generated by a two-photon process non-adiabatically [20]. Similarly, the generation and stabilization of cat state based on the interplay between Kerr nonlinearity and single-mode squeezing has been demonstrated experimentally [21]. A review work provides a comprehensive perspective about quantum amplification and simulation for strong and ultrastrong coupling of light and matter [22]. We will combine the time-dependent two-photon processes with a reinforcement learning module to prepare non-classical quantum states in this work.

Machine-learning techniques are emerging as effective tools in exploring physics [23–26], and among them, reinforcement learning (RL) has the potential to find optimal control fields to engineer system dynamics, given that the evolution of these systems is governed by specific differential equations. Time-varying control proposals has been employed to produce spin squeezing in a collective spin systems [27, 28]. These works establishes a foundational framework to generate specific quantum states by reinforcement learning. Reinforcement learning can successfully steer the quantum Kapitza oscillator to a Floquet-engineered stable inverted position amidst noise, with applications in quantum information and quantum optics[29].

We first exhibit the phase diagram of a two-photon-driven quantum Rabi model to delineate the parameter region to work on. Then we mainly propose an RL-based control scheme to design the time-varying amplitudes of the two-photon-driven strength to enhance the entanglement between the qubit and cavity mode. The agent is trained to produce a sequence of 3-value square pulses to steer the system to entangled states under the domain of a Lindblad master equation at strong coupling regimes and the critical point for different initial states.

This paper is organized as follows: In Sec.II, we introduce the two-photon-driven Rabi model. In Sec.III, the phase diagram versus the coupling strength and two-photon-driven amplitudes in terms of several quantities are given. In Sec.IV, we present the procedure to en-

[†] These authors should be considered co-first authors.

hance entanglement via reinforcement learning, including reinforcement learning, dynamics and control results. In Sec.V, we discuss the generalization of this control scheme in terms of the controlled quantum system and the replaceability of the reinforcement learning module. Finally, we conclude in Sec.VI.

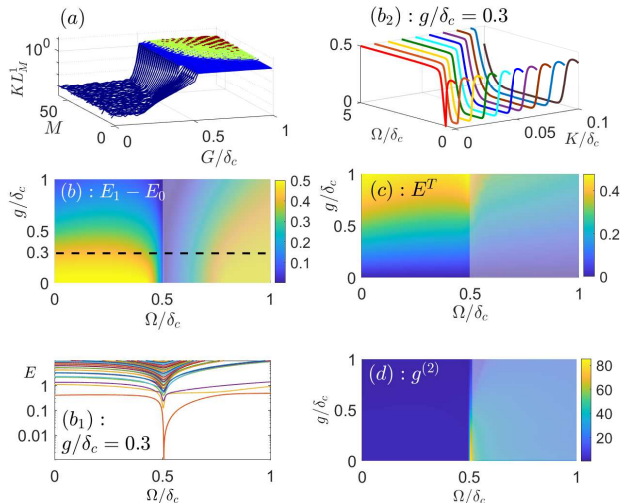


FIG. 1. (a) KL_M^1 versus the truncated dimension M and Ω/δ_c when $g/\delta_c = 0.1$ (logarithmic scale used). (b) The energy gap between the first excited state E_1 and the ground state E_0 versus g/δ_c and Ω/δ_c , $M = 60$ and $K/\delta_c = 0$ hereafter. (b1) The energy spectrum $E - E_0$ versus Ω/δ_c when $g/\delta_c = 0.3$. (b2) The energy gap $E_1 - E_0$ versus Ω/δ_c and K/δ_c when $g/\delta_c = 0.3$. (c) The partial transposed criteria for entanglement of the ground state ρ_0 , denoted by E^T versus g/δ_c and Ω/δ_c . (d) Equal time second order correlation versus g/δ_c and Ω/δ_c . Areas where numerical simulations might fail are overlaid with a white semi-transparent shadow.

II. THE MODEL

Quantum Rabi model [1, 2] describes the interaction between a single-mode bosonic field (such as a cavity mode) and a qubit (generic two-state system). It is described by the Hamiltonian ($\hbar = 1$ hereafter)

$$\hat{H} = \delta_c \hat{a}^\dagger \hat{a} + \frac{\delta_q}{2} \hat{\sigma}_z + g(\hat{a} + \hat{a}^\dagger)(\hat{\sigma}_- + \hat{\sigma}_+) + \Omega(\hat{a}^2 + \hat{a}^{\dagger 2}) + K\hat{a}^{\dagger 2}\hat{a}^2, \quad (1)$$

where \hat{a}^\dagger (\hat{a}) is the creation (annihilation) operator for the bosonic cavity mode and $\hat{\sigma}_z$ is the Pauli z -basis operator with commute relation $[\hat{\sigma}_+, \hat{\sigma}_-] = \hat{\sigma}_z$. $\delta_{c(q)} = \omega_{c(q)} - \omega_p$, where ω_c , ω_q and ω_p are the frequencies of the cavity, qubit and parametrical driving, respectively. The parameter g is the coupling strength between the two subsystems. The two-photon parameter driven term $\Omega(\hat{a}^2 + \hat{a}^{\dagger 2})$ can be implemented by Kerr nonlinear Hamiltonian [16–21].

In the regime of weak coupling, through the rotating wave approximation, the quantum Rabi model can be effectively described by the Jaynes-Cummings model [30], which has been investigated widely in circuit QED system [14], cavity QED system [31], and trapped ions [32, 33]. When the coupling strength approaches or surpasses the frequency scales of the cavity mode and the qubit, the rotating wave approximation no longer holds and remarkable phenomena emerge [34]. We will examine the phase diagram with respect to the two-photon-driven strength and the coupling rate between the subsystems. Then the dynamical behavior to enhance the entanglement by reinforcement learning method is investigated.

III. THE PHASE DIAGRAM

If a system has different phases, it possesses distinguishable properties in different phases. We conjecture there is a phase transition in the two-photon-driven Rabi model, which may be examined by the behavior of several quantities versus the strength of the parameter-driven amplitude Ω/δ_c and coupling strength g/δ_c in the Hamiltonian (1). In addition to the energy gap between the ground state and the first excited state, the partial transpose criteria for entanglement, second correlation, and negative value of Wigner function are checked in Fig. 1 and Fig. 2.

The number of excitations in the cavity field in the ground state may increase dramatically as the parameters in the Hamiltonian vary. In order to ensure the accuracy of numerical simulations, a higher truncation dimension is required. To ensure the accuracy of numerical simulations, inspired by the concept of Kullback-Leibler divergence (relative entropy) [35], we define a quantity denoted as KL_M^q :

$$KL_M^q = \rho_{M+q} |\log \rho_{M+q} - \log \rho_M|, \quad (2)$$

where ρ_M is the density matrix for the ground state of dimension- M eigenspace and the integer q represents the dimension difference between the two density matrices. 0-padding is used at the higher truncation margin of the density matrix ρ_M to compensate for the truncation difference between ρ_M and ρ_{M+q} . When calculating the logarithm of the matrix elements, 0 matrix elements will be replaced by 1. This metric is used to quantify the difference of ρ_M and ρ_{M+q} . A smaller value of KL_M^q indicates a larger similarity between the two states. As shown in Fig. 1 (a) with $K/\delta_c = 0$, KL_M^1 diverges when $\Omega/\delta_c > 0.5$. This divergence behavior of KL_M^1 occurs with the continuous change of Ω/δ_c , so

$$\Omega_c = \frac{\delta_c}{2}. \quad (3)$$

is a critical point for a phase transition. Thus we will investigate the dynamics in the regime $\Omega/\delta_c \leq 0.5$.

This phase transition can also be indicated by the energy gap between the first excited state and the ground

state of the Hamiltonian (1) as shown in Fig. 1 (b). As shown in (b₁), the energy spectrum exhibits a tendency towards degeneracy at Ω_c . These results coincide with the that in Fig. 1 (a). The Kerr nonlinearity K in the Hamiltonian (1) can be seen as a kind of photon-dependent photon number shift [16–21]. The influence of this Kerr nonlinearity on $E_q - E_0$ can be seen in Fig. 1(b₂). With increasing of K/δ_c , the energy gap $E_1 - E_0$ extends. In this work, we focus on the dynamical character while enhancing entanglement by machine learning with $K/\delta_c = 0$.

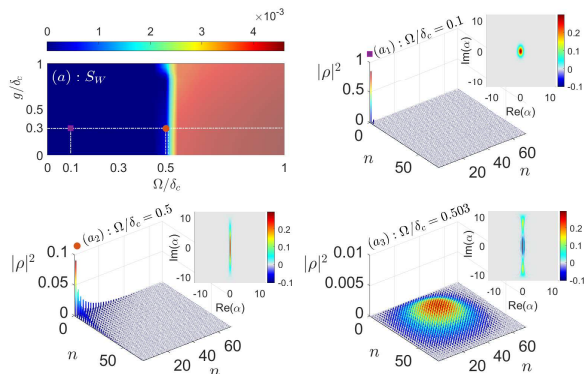


FIG. 2. (a) The average of evenly distributed 10000 sampling points of the Wigner function versus g/δ_c and Ω/δ_c for the cavity ground state. (a₁) - (a₃) The distribution of $|\rho|^2$ for the cavity ground states when the coupling strength $g/\delta_c = 0.3$ and $\Omega/\delta_c = 0.3, 0.5, 0.503$ with the corresponding Wigner functions, respectively.

The partial transpose criterion involves analyzing the eigenvalues of the partially transposed density matrix of the composite system, and it offers a sufficient (but not necessary) criterion for witnessing entanglement in bipartite quantum systems [36, 37]. The appearance of negative eigenvalues of the partially transposed density matrix is definitely a signature of entanglement. The absolute of the negative eigenvalues of the partially transposed density matrix (denoted by λ_i) are summarized to act as the entanglement witness:

$$E^T = \sum_{\lambda_i < 0} |\lambda_i|. \quad (4)$$

As shown in Fig. 1(c), the phase diagram indicated by E^T coincides with the results in Fig. 1 (a) and (b).

In the strong and ultra-strong coupling regimes, to exclude unphysical quadrature measurements, an effective approach for describing the system involves solving the eigen-equations of the Hamiltonian (1) to construct the dressed space. Then the cavity-field operators are redefined with positive and negative frequencies. $\hat{X}^+ = \sum_{j,k>j} X_{jk}|j\rangle\langle k|$ and $\hat{X}^- = (\hat{X}^+)^{\dagger}$, with $X_{jk} \equiv \langle j|\hat{a}^{\dagger} + \hat{a}|k\rangle$, in the dressed eigen-basis $|j\rangle, |k\rangle$

of the Hamiltonian (1) with eigen-values ω_j and ω_k , respectively [38, 39]. In the limit of weak coupling, these operators coincide with \hat{a} and \hat{a}^{\dagger} , respectively. And similar operators can be defined for $\hat{\sigma}_-$ and $\hat{\sigma}_+$ [38, 39]. The master equation when applied to describe the dynamics, would be modified by these dressed operators.

The strong correlation of emitted photons can now be decided by the equal time second order correlation defined as

$$g^{(2)} = \frac{\langle \hat{X}^{+2} \hat{X}^2 \rangle}{\langle \hat{X}^+ \hat{X} \rangle^2}. \quad (5)$$

The behavior of $g^{(2)}$ versus Ω/δ_c and g/δ_c is shown in Fig. 1(d) coincides the phase transition in Fig. 1(a).

To gain insight into the phase transition further, we examine the Wigner function of the ground states versus system parameters. The appearance of negative values in the Wigner function is a sufficient but not necessary condition for characterizing the non-classicality of a quantum state. We use the average of the negative values of the Wigner function as

$$S_W = \frac{1}{M} \sum_n W_{<0} \quad (6)$$

to show the non-classicality of the cavity state, where $W_{<0}$ are the negative values of M evenly distributed sampling point of the Wigner function. S_W versus Ω/δ_c and g/δ_c is shown in Fig. 2(a). The sudden change of S_W confirms the phase transition in Eq. (3). The Wigner functions of the ground state in different phases are shown in Fig. 2(a₁), (a₂) and (a₃) with the density matrices $|\rho|^2$ of the cavity ground states. Upon $\Omega/\delta_c > \Omega_c$, S_W changes abruptly with negative texture in Wigner function emerges. Meanwhile, the distribution of $|\rho|^2$ versus the index of the basis n , changes obviously.

IV. ENHANCE ENTANGLEMENT BY REINFORCEMENT LEARNING

Taking a cue from control strategies by Lyapunov control and machine learning [40, 41], we propose a scheme harnessing an RL agent to design temporal control field to enhance the entanglement and check the influence of system parameters. Drawing inspiration from time-dependent parameter process [16–21], in this control proposal, the Hamiltonian for the controlled quantum system reads:

$$\hat{H} = \delta_c \hat{a}^{\dagger} \hat{a} + \frac{\delta_q}{2} \hat{\sigma}_z + g(\hat{a} + \hat{a}^{\dagger})(\hat{\sigma}_- + \hat{\sigma}_+) + \Omega(t)(\hat{a}^2 + \hat{a}^{\dagger 2}), \quad (7)$$

here $\Omega(t) = \Omega_{max} f(t)$ with $f(t)$ is the control sequence designed by the RL agent, and Ω_{max} is the amplitude. In this control process, $[\hat{a}^{\dagger} \hat{a} + \hat{\sigma}_z + (\hat{a} + \hat{a}^{\dagger})(\hat{\sigma}_- + \hat{\sigma}_+), \hat{a}^2 + \hat{a}^{\dagger 2}] \neq 0$ ensures the effectiveness of the control fields.

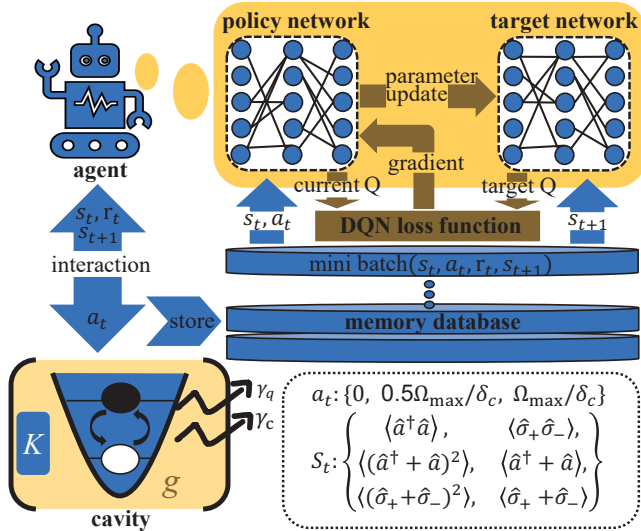


FIG. 3. The workflow of using reinforcement learning agent to enhance the entanglement for the two-photon-driven Rabi model.

The workflow for this control scheme is illustrated in Fig. 3. The control field $\Omega(t)$ acts as the sequence of the actions and the increase of E^T is positively related with the reward function in the reinforcement learning.

A. Reinforcement Learning

Starting with no prior knowledge about the system under control, RL uses the trial-and-error paradigm to iteratively learn the mapping between actions and states that maximizes the accumulated reward over time. An appropriate rewards-evaluation rule that favors particular state-action mappings which can enhance the control performance. Decision-making executed by the agent entails selecting actions $a_t = \pi(s_t)$ that manipulates the system changing from a state (not referring to quantum states, but a set of expectations of operators of the controlled system) s_t to s_{t+1} , with π denoting the policy being learned [23, 24].

Q -learning operates through a Q function that represents the expected total future reward for a given policy π [42, 43]. The optimal policy π^* with the maximized Q function satisfies Bellman equation which encapsulates the principle of optimality for decision-making over time. Deep Q -learning network (DQN) has been proposed to approximate this function [44–48].

B. Enhancing entanglement by machine-designed pulses

In DQN, the reward function is designed with the aim of achieving the control objective. In our reinforcement learning proposal, the entanglement witness is employed

to establish the reward function. In this work, the reward function we employ is

$$R_t = 10 \langle \Delta E_t^T > 0 \rangle - \langle \Delta E_t^T \leq 0 \rangle, \quad (8)$$

where $\langle \bullet \rangle$ is the sign function of \bullet and $\Delta E_t^T = E_{(t+1)}^T - E_{(t)}^T$. Here $E_{(t)}^T$ is the partial transpose criterion for entanglement at discrete sampling time t . This means the agent gets 10 points of reward when the entanglement increases and deducts 1 point when the entanglement decreases. This is consistent with the core principles of reinforcement learning, the agent is incentivized to provide actions to steer the system towards states with higher entanglement.

In this work, the RL agent selects those actions a_t at sampling time t , contingent upon the observations $S_t = \{ \langle \hat{a}^\dagger \hat{a} \rangle, \langle \hat{\sigma}_+ \hat{\sigma}_- \rangle, \langle (\hat{a}^\dagger + \hat{a})^2 \rangle, \langle \hat{a}^\dagger + \hat{a} \rangle, \langle (\hat{\sigma}_+ + \hat{\sigma}_-)^2 \rangle, \langle \hat{\sigma}_+ + \hat{\sigma}_- \rangle \}$, thereby orchestrating a sequence of actions consist of $a_t \in \{0, 0.5\Omega_{max}/\delta_c, \Omega_{max}/\delta_c\}$ aimed at maximizing cumulative rewards and minimizing penalties based on R_t . During the training, the observations are fed into the neural network, while output neurons provide the probability of choosing which action at the next iterative training step. A reward is dispensed subsequently to each step to evaluate the decision-making policy. After one epoch, the controlled system is re-initialized to the same initial state and the next epoch starts to train the agent continuously based on the trained neural network. The state evolves according to the environment dynamics, which is deterministic (9). The learned policy π^* is represented by the arrangement of the pulse sequences.

It is necessary to take measures to optimize the performance of reinforcement learning. One is introducing the replay structure, which stores past experiences during training to improve both learning efficiency and stability. To enhance the robustness of the reinforcement learning agent against large errors resulting from the use of linear functions, the Huber loss is employed [49]. This loss function not only avoids underestimating or overestimating the influence of small errors, but also helps to mitigate the exploding gradient problem during the training of deep neural networks, which benefits convergence compared to other loss functions [49]. The neural network parameters are updated by the algorithm AdamW [50] which applies the decay directly to the weights. It is beneficial in suppressing overfitting. Yet, Huber loss and AdamW can be replaced by other loss functions and optimization algorithms [23, 24]. The inherent randomness in the reinforcement learning algorithm introduces a probability that enables the agent to explore and identify the most effective sequence of actions.

It is essential to emphasize that the proposed strategy operates within a closed-loop framework during simulation, while the actual implementation follows an open-loop control scheme. Once the control sequence for $\Omega(t)$ in the Hamiltonian (1) is obtained through simulation, the same control field is applied in an open-loop process to avoid quantum collapse caused by direct observation on the system.

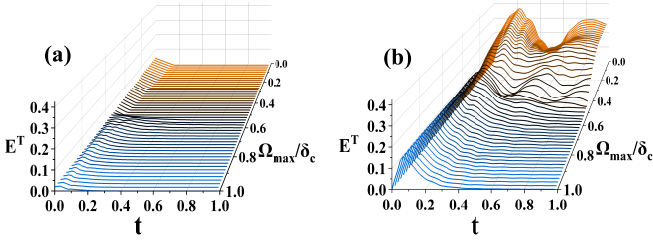


FIG. 4. Evolution of the entanglement indicated by partial transposed criterion E^T versus the amplitude of the two-photon-driven parameter Ω_{max} for the initial state $\rho(0) = \rho_0$ is the ground state of the Hamiltonian (1) in (a), and $\rho(0) = |\alpha = 1, \downarrow\rangle\langle\alpha = 1, \downarrow|$ in (b). $\delta_q/\delta_c = 1$, $g/\delta_c = 0.3$, $K/\delta_c = 0$, and the dissipation rates $\gamma_c/\delta_c = \gamma_q/\delta_c = 0.01$.

C. Entanglement dynamics in open conditions

Usually, it is hard to avoid decoherence in a quantum system due to its interaction with the environment. The effect of such decoherence should be taken into account in this control scheme to ensure reliability. There are two kinds of decoherence channels: dissipation of the cavity field and the qubit, which ruin the entanglement. The system would evolve under the domain of the Lindblad master equation with the application of the time-dependent two-photon-driven term $\Omega(t) = \Omega_{max}f(t)$ in the Hamiltonian (1) designed using reinforcement learning.

In the strong and ultrastrong coupling regimes, the realistic scenarios with the environment temperature T , is described by the master equation

$$\dot{\rho}(t) = i[\rho(t), \hat{H}] + \mathcal{L}_{\hat{a}}\rho(t) + \mathcal{L}_{\hat{\sigma}_-}\rho(t), \quad (9)$$

where $\mathcal{L}_{\hat{a}}$ and $\mathcal{L}_{\hat{\sigma}_-}$ are Liouvillian superoperators describing the decoherence of the cavity field and qubit [51]. They read $\mathcal{L}_{\hat{\chi}}\rho(t) = \sum_{j,k>j} \Gamma_{\hat{\chi}}^{jk} \bar{n}(\Delta_{kj}, T) \mathcal{D}[|k\rangle\langle j|]\rho(t) + \sum_{j,k>j} \Gamma_{\hat{\chi}}^{jk} (1 + \bar{n}(\Delta_{kj}, T)) \mathcal{D}[|j\rangle\langle k|]\rho(t)$ for $\hat{\chi} = \hat{a}(\hat{\sigma}_-)$ represents the cavity field (qubit), $\mathcal{D}[\mathcal{O}]\rho(t) = \frac{1}{2}(2\mathcal{O}\rho(t)\mathcal{O}^\dagger - \rho(t)\mathcal{O}^\dagger\mathcal{O} - \mathcal{O}^\dagger\mathcal{O}\rho(t))$. The relaxation coefficients $\Gamma_{\hat{\chi}}^{jk} = 2\pi d(\Delta_{kj}) \alpha_{\hat{\chi}}^2(\Delta_{kj}) |C_{jk}^{\hat{\chi}}|^2$ with $d(\Delta_{kj})$ being the spectral density of the baths, $\alpha_{\hat{\chi}}(\Delta_{kj})$ denoting the system-bath coupling strength, $\Delta_{kj} = \omega_k - \omega_j$, and $C_{jk}^{\hat{\chi}} = -i\langle j | (\hat{\chi} - \hat{\chi}^\dagger) | k \rangle$. $\bar{n}(\Delta_{kj}, T)$ (\bar{n} for short) is the thermal population at frequency Δ_{kj} with environment temperature T . When considering a cavity coupling to the momentum quadrature of a field in one-dimension waveguides, the spectral density $d(\Delta_{kj})$ is constant and $\alpha_{\hat{\chi}}^2(\Delta_{kj}) \propto \Delta_{kj}$. Then the relaxation coefficients reduce to $\Gamma_{\hat{\chi}}^{jk} = \gamma_{\hat{\chi}}(\Delta_{kj}/\omega_0) |C_{jk}^{\hat{\chi}}|^2$ where $\gamma_{\hat{\chi}}$ is the damping rate. These assumptions can be realized in circuit-QED. The influence of dephasing and Lamb shifts in current experiments can be deemed negligible as they do not exert significant influence [32, 33].

In this study, we put forward a conjecture that the dy-

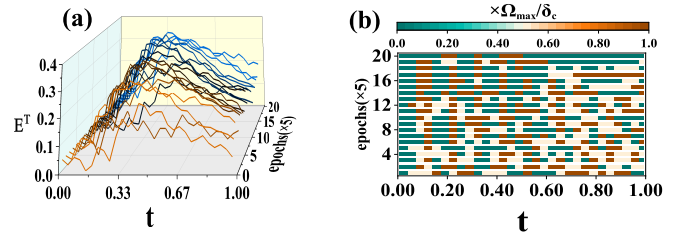


FIG. 5. (a) The dynamics of the entanglement indicated by E^T versus the training epoches. (b) The corresponding square control pulses $\Omega(t)$ ($\Omega_{max}/\delta_c = 0.3$) from the top view, with values shown in the color bar. $\rho(0) = \rho_0$ is the ground state of the Hamiltonian (1), $\delta_q/\delta_c = 1$, $g/\delta_c = 0.3$, $K/\delta_c = 0$, and dissipation rates $\gamma_{\hat{a}}/\delta_c = \gamma_{\hat{\sigma}_-}/\delta_c = 0.01$.

namics of the entanglement can reflect the phase transition for different initial states. We first check the dynamics of the entanglement versus the constant two-photon-driven strength when $g/\delta_c = 0.3$ in Fig. 4. As shown in Fig. 4 (a), the strength and duration time of the entanglement for the ground state decreases as Ω/δ_c increases. This character coincides with the results in Fig. 1 (c). This means constant two-photon process has a negative effect on the entanglement. While the initial state $\rho(0) = |\alpha = 1, \downarrow\rangle\langle\alpha = 1, \downarrow|$, where $|\alpha = 1\rangle$ is the coherent state with amplitude 1, the entanglement exhibits more fluctuations versus time when Ω_{max}/δ_c is below the phase critical point Ω_c . Comparing Fig. 4 (a) and (b), the entanglement increases more obviously when the initial state is the non-entangled product state than the entangled ground state.

D. Entanglement under control

We check the dynamics of the entanglement witness E^T under the control versus different system parameters and initial states. The time interval $[0, 1]$ is partitioned into 30 segments of control square pulses with amplitudes picked in $\{0, 0.5\Omega_{max}/\delta_c, \Omega_{max}/\delta_c\}$ determined by the RL agent. The RL agent designs the arrangement of the pulses under the objective of increasing the entanglement. Each round of the training consists of 100 epochs. As an example, one round of the control process to find the sequence of square pulses is shown in Fig. 5. As shown in Fig. 5(a), along with the training, the RL agent can find numerous sequences of square pulses all with increased entanglement. The corresponding control sequences are shown in Fig. 5(b). This control method can be regarded as a kind of combination of bang-bang control [52, 53] and reinforcement learning. From a statistical view, it can be intuitively observed that as learning progresses, the probability of $\Omega_{max}/\delta_c = 0$ decreases in the distribution of the control pulses. These solutions corroborate the efficacy of the control pulses designed by the RL agent to enhance the generation of entanglement.

Zero temperature was assumed in the previous results.

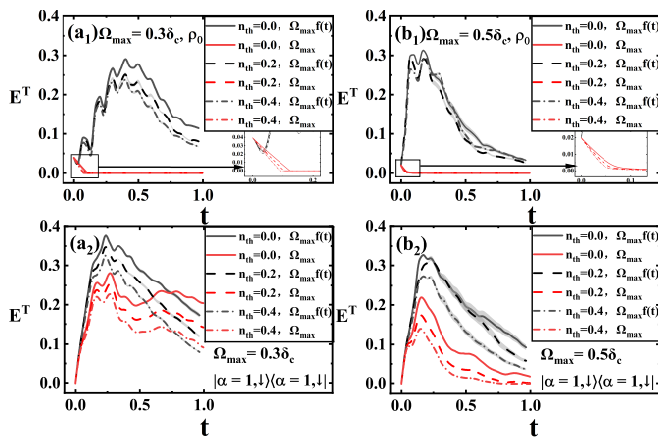


FIG. 6. The average evolutions of 20 entanglement criterion E^T with error zones for different two-photon-driven amplitudes and initial states. (a₁) $\Omega_{max} = 0.3\delta_c$ and $\rho(0) = \rho_0$, the ground state of the Hamiltonian (1). (a₂) $\Omega_{max} = 0.3/\delta_c$ and $\rho(0) = |\alpha = 1, \downarrow\rangle\langle\alpha = 1, \downarrow|$. (b₁) $\Omega_{max} = 0.5\delta_c$ and $\rho(0) = \rho_0$ is the ground state of the Hamiltonian (1). (b₂) $\Omega_{max} = 0.5\delta_c$ and $\rho(0) = |\alpha = 1, \downarrow\rangle\langle\alpha = 1, \downarrow|$. The other parameters are same to those in Fig. 5.

To investigate the robustness of the protocol in reality, it is natural to consider the influence of temperature on the control results. Since $\bar{n} = \frac{1}{\exp^{\hbar\omega/k_B T} - 1}$, the average number of thermal excitations in the reservoir \bar{n} is positively correlated to the temperature T and the strength of the decoherence according to the master equation (9). To examine the influence of temperature on the control effect at different system parameters and initial states, we show the dynamics of E^T at different \bar{n} s in Fig. 6. From a statistical perspective, larger \bar{n} is detrimental to the enhancement of entanglement, whether or not the proactive control by RL is applied to the system. From a holistic perspective, the application of the control field designed by the RL agent has a positive effect on enhancing the entanglement. By comparing (a₁) with (a₂) ($\Omega_{max}/\delta_c = 0.3$), or (b₁) with (b₂) ($\Omega_{max}/\delta_c = 0.5$), the entanglement dynamics become similar when the control is applied. And the entanglement can be enhanced more obviously by the control when the initial state is the entangled ground state. By comparing (a₁) with (b₁), or (a₂) with (b₂), larger two-photon-driven strength is detrimental to the production of entanglement. At the critical point, i.e., $\Omega_{max}/\delta_c = 0.5$, the negative impact of temperature on entanglement enhancement is not significant enough. In this control scheme, it is reasonable that one should choose the best control sequence among the solutions.

V. GENERALIZATION CAPABILITY OF THE SCHEME

The RL agent finds solutions to optimization problems through a trial-error mechanism based on statistical principles. In a quantum-well waveguide system, the light-matter interaction can be turned from weak to ultrastrong within less than one cycle of light [54], which provides the probability to implement this control scheme. The tunability of the single-photon strong-coupling strength may be the candidate to produce quantum squeezing [55]. In a word, any other systems under certain mapping rules (such as differential equations) with tunable parameters can be considered as the controlled system in this proposal. Not only the controlled system but also the RL agent can be replaced by other RL modules that perform similar functions. For example, several alternatives have been identified and evaluated, including the State-Action-Reward-State-Action algorithm [45], Deep Deterministic Policy Gradient [46], Asynchronous Advantage Actor-Critic [47], and the Dueling Network [48] and so on.

VI. CONCLUSION

In a Rabi model driven by a two-photon parameter, besides the energy gap between the first excited state and the ground state, the entanglement criterion, equal-time second-order correlation, and negativity of the Wigner function in the ground state also reflect the phase transition. The entanglement dynamics exhibits a significant change at the critical boundary. The reinforcement learning agent was employed to design a suite of square pulses to modulate the time-varying two-photon parameter strength, thereby enhancing the entanglement dynamically in an open environment. The entanglement is still enhanced, despite stronger dissipation impairs more severely to the control performance. The versatility of the control scheme is demonstrated by the potential to substitute the reinforcement learning agent with other optimization modules and replace the controlled system with other systems that have tunable parameters. This work provides the avenue to study non-equilibrium control problems using reinforcement learning agents.

VII. ACKNOWLEDGEMENTS

X. L. Zhao thanks discussions with Wenzhao Zhang, Natural Science Foundation of Shandong Province, China, No.ZR2020QA078, No.ZR2023MD064, ZR2022QA110, and National Natural Science Foundation of China, No.12005110.

[1] I. I. Rabi, Space quantization in a gyrating magnetic field, Phys. Rev. **51**, 652 (1937).

[2] H. Walther, B. T. H. Varcoe, B. G. Englert, and T. Becker, Cavity quantum electrodynamics, Rep. Prog.

- Phys. **69**, 1325 (2006).
- [3] S. Haroche, and J. -M. Raimond, Exploring the Quantum: Atoms, Cavities, and Photons, Oxford University Press (2006).
 - [4] P. Forn-Díaz, L. Lamata, E. Rico, J. Kono, and E. Solano, Ultrastrong coupling regimes of light-matter interaction, Rev. Mod. Phys. **91**, 025005 (2019).
 - [5] F. Yoshihara, T. Fuse, Z. Ao, S. Ashhab, K. Kakuyanagi, S. Saito, T. Aoki, K. Koshino, and K. Semba, Inversion of Qubit Energy Levels in Qubit-Oscillator Circuits in the Deep-Strong-Coupling Regime, Phys. Rev. Lett. **120**, 183601 (2018).
 - [6] S. Ashhab, Superradiance transition in a system with a single qubit and a single oscillator, Phys. Rev. A **87**, 013826 (2013).
 - [7] M. J. Hwang, R. Puebla, and M. B. Plenio, Quantum Phase Transition and Universal Dynamics in the Rabi Model, Phys. Rev. Lett. **115**, 180404 (2015).
 - [8] S. Ashhab, and F. Nori, Qubit-oscillator systems in the ultrastrong-coupling regime and their potential for preparing nonclassical states, Phys. Rev. A **81**, 042311 (2010).
 - [9] C. Leroux, L. C. G. Góvia, and A.A. Clerk, Simple variational ground state and pure-cat-state generation in the quantum Rabi model, Phys. Rev. A **96**, 043834 (2017).
 - [10] K. Gietka, C. Hotter, and H. Ritsch, Unique Steady-State Squeezing in a Driven Quantum Rabi Model, Phys. Rev. Lett. **131**, 223604 (2023).
 - [11] T. Niemczyk, F. Deppe, H. Huebl, E. P. Menzel, F. Hocke, M. J. Schwarz, J. J. García-Ripoll, D. Zueco, T. Hummer, E. Solano, A. Marx, and R. Gross, Circuit quantum electrodynamics in the ultrastrong-coupling regime, Nat. Phys. **6**, 772 (2010).
 - [12] F. Yoshihara, T. Fuse, S. Ashhab, K. Kakuyanagi, S. Saito, and K. Semba, Superconducting qubit-oscillator circuit beyond the ultrastrong-coupling regime, Nat. Phys. **13**, 44 (2017).
 - [13] J. Braumüller, M. Marthaler, A. Schneider, A. Stehli, H. Rotzinger, M. Weides, and A. V. Ustinov, Analog quantum simulation of the Rabi model in the ultra-strong coupling regime, Nat. Commun. **8**, 779 (2017).
 - [14] D. Ballester, G. Romero, J. J. García-Ripoll, F. Deppe, and E. Solano, Quantum Simulation of the Ultrastrong-Coupling Dynamics in Circuit Quantum Electrodynamics, Phys. Rev. X **2**, 021007 (2012).
 - [15] A. Wallraff, D. I. Schuster, A. Blais, L. Frunzio, R.S. Huang, J. Majer, S. Kumar, S. M. Girvin, and R. J. Schoelkopf, Strong coupling of a single photon to a superconducting qubit using circuit quantum electrodynamics, Nature **431**, 162 (2004).
 - [16] G. J. Milburn, and C. A. Holmes. Quantum coherence and classical chaos in a pulsed parametric oscillator with a Kerr nonlinearity. Phys. Rev. A **44**, 4704 (1991).
 - [17] W. Qin, A. Miranowicz, P.-B. Li, X.-Y. Lü, J.Q. You, and F. Nori, Exponentially enhanced light-matter interaction, cooperativities, and steady-state entanglement using parametric amplification, Phys. Rev. Lett. **120**, 093601 (2018).
 - [18] C. Leroux, L. C. G. Góvia, and A. A. Clerk, Enhancing Cavity Quantum Electrodynamics via Antisqueezing: Synthetic Ultrastrong Coupling, Phys. Rev. Lett. **120**, 093602 (2018).
 - [19] C. J. Zhu, L. L. Ping, Y. P. Yang, and G. S. Agarwal, Squeezed Light Induced Symmetry Breaking Super-radiant Phase Transition, Phys. Rev. Lett. **124** 073602 (2020).
 - [20] S. Puri, S. Boutin, and A. Blais, Engineering the quantum states of light in a Kerr-nonlinear resonator by two-photon driving, npj Quantum Inf. **3**, 18 (2017).
 - [21] A. Grimm, N. E. Frattini, S. Puri, S. O. Mundhada, S. Touzard, M. Mirrahimi, S. M. Girvin, S. Shankar, and M. H. Devoret, Stabilization and operation of a Kerr-cat qubit, Nature, **584**, 205 (2020).
 - [22] W. Qin, A. F. Kockum, C. S. Muñoz, A. Miranowicz, and F. Nori, Quantum amplification and simulation of strong and ultra-strong coupling of light and matter, Physics Reports **1078**, 1(2024)
 - [23] K. P. Murphy, Machine Learning: A Probabilistic Perspective, MIT Press (2012).
 - [24] R. S. Sutton, and A. G. Barto, Reinforcement learning: An introduction, MIT Press (2018).
 - [25] T. Fösel, P. Tighineanu, T. Weiss, and F. Marquardt, Reinforcement learning with neural networks for quantum feedback, Phys. Rev. X **8**, 031084 (2018).
 - [26] V. Dunjko, and H. J. Briegel, Machine learning artificial intelligence in the quantum domain: a review of recent progress, Reports on Progress in Physics **81**, 074001 (2018).
 - [27] Q. S. Tan, M. Zhang, Y. Chen, J. Q. Liao, and J. Liu, Generation and storage of spin squeezing via learning-assisted optimal control, Phys. Rev. A **103**, 032601 (2021).
 - [28] X. L. Zhao, Y. M. Zhao, M. Li, T. T. Li, Q. Liu, S. Guo, and X. X. Yi, A Strategy for Preparing Quantum Squeezed States Using Reinforcement Learning, Annalen der Physik **536**. 2400056 (2024).
 - [29] M. Bukov, Reinforcement learning for autonomous preparation of Floquet-engineered states: Inverting the quantum Kapitza oscillator, Phys. Rev. B **98**, 224305 (2018).
 - [30] R. Miller, T. E. Northup, K. M. Birnbaum, A. D. B. A. Boca, A. D. Boozer, and H. J. Kimble, Trapped atoms in cavity QED: coupling quantized light and matter, J. Phys. B **38**, S551 (2005).
 - [31] J. M. Raimond, M. Brune, and S. Haroche, Manipulating quantum entanglement with atoms and photons in a cavity, Rev. Mod. Phys. **73**, 565 (2001).
 - [32] R. Puebla, M. J. Hwang, J. Casanova, and M. B. Plenio, Probing the Dynamics of a Superradiant Quantum Phase Transition with a Single Trapped Ion, Phys. Rev. Lett. **118**, 073001 (2017).
 - [33] Q. X. Mei, B. W. Li, Y. K. Wu, M. L. Cai, Y. Wang, L. Yao, Z. C. Zhou, and L. M. Duan, Experimental Realization of the Rabi-Hubbard Model with Trapped Ions, Phys. Rev. Lett. **128**, 160504 (2022).
 - [34] A. F. Kockum, A. Miranowicz, S. De Liberato, S. Savasta, and F. Nori, Ultrastrong coupling between light and matter. Nat Rev Phys **1**, 19 (2019).
 - [35] S. Kullback, and R. A. Leibler, On Information and Sufficiency, Annals of Mathematical Statistics, **22**, 79 (1951).
 - [36] G. Vidal, and R. F. Werner, Computable measure of entanglement, Phys. Rev. A **65**, 032314 (2002).
 - [37] A. Peres, Separability Criterion for Density Matrices, Phys. Rev. Lett. **77**, 1413 (1996).
 - [38] L. Garziano, A. Ridolfo, R. Stassi, O. Di Stefano, and S. Savasta, Switching on and off of ultrastrong light-matter interaction: Photon statistics of quantum vacuum radiation, Phys. Rev. A **88**, 063829 (2013).

- [39] L. Garziano, R. Stassi, V. Macrì, A. F. Kockum, S. Savasta, and F. Nori, Multiphoton quantum Rabi oscillations in ultrastrong cavity QED, *Phys. Rev. A* **92**, 063830 (2015).
- [40] X. L. Zhao, Y. L. Ma, H. Y. Ma, T. H. Qiu, and X. X. Yi, Prepare non-classical collective spin state by designing control fields, *Physics Lett A* **425**, 127874 (2022).
- [41] X. L. Zhao, Y. M. Zhao, M. Li, T. T. Li, Q. Liu, S. Guo, and X. X. Yi, A Strategy for Preparing Quantum Squeezed States Using Reinforcement Learning, *Annalen der Physik*: 2400056 (2024)
- [42] V. Mnih, K. Kavukcuoglu, D. Silver, A. A. Rusu, J. Veness, M. G. Bellemare, A. Graves, M. Riedmiller, A. K. Fidjeland, G. Ostrovski, S. Petersen, C. Beattie, A. Sadik, I. Antonoglou, H. King, D. Kumaran, D. Wierstra, S. Legg, and D. Hassabis, Human-level control through deep reinforcement learning, *Nature* **518**, 529 (2015).
- [43] R. Bellman, On the theory of dynamic programming, *Proc. Natl. Acad. Sci.* **38**, 716 (1952).
- [44] Y. LeCun, Y. Bengio, and G. Hinton, Deep learning, *Nature* **521**, 436 (2015).
- [45] G. A. Rummery, and M. Niranjan, <https://api.semanticscholar.org/CorpusID:59872172> (1994).
- [46] D. Silver, G. Lever, N. Heess, T. Degris, D. Wierstra, and M. Riedmiller, Proceedings of the 31st International Conference on Machine Learning, PMLR **32**, 387 (2014).
- [47] V. Mnih, A. P. Badia, M. Mirza, A. Graves, T. P. Lillicrap, T. Harley, D. Silver, and K. Kavukcuoglu, arXiv:1602.01783 (2016).
- [48] Z. Wang, T. Schaul, M. Hessel, H. v. Hasselt, M. Lanctot, and N. d. Freitas, Proceedings of The 33rd International Conference on Machine Learning, PMLR **48**, 1995 (2016).
- [49] P. J. Huber, *Annals of Mathematical Statistics* **35**, 73 (1964).
- [50] I. Loshchilov, Decoupled weight decay regularization, arXiv preprint arXiv:1711.05101 (2017).
- [51] F. Beaudoin, J. M. Gambetta, and A. Blais, Dissipation and ultrastrong coupling in circuit QED, *Phys. Rev. A* **84**, 043832 (2011).
- [52] L. Viola, and S. Lloyd, Dynamical suppression of decoherence in two-state quantum systems, *Phys. Rev. A* **58**, 2733 (1998).
- [53] S. C. Hou, M. A. Khan, X. X. Yi, D. Dong, and I. R. Petersen, Optimal Lyapunov-based quantum control for quantum systems, *Phys. Rev. A* **86**, 022321 (2012).
- [54] G. Günter, A. A. Anappara, J. Hees, A. Sell, G. Biasiol, L. Sorba, S. De Liberato, C. Ciuti, A. Tredicucci, A. Leitenstorfer, and R. Huber, Sub-cycle switch-on of ultrastrong light-matter interaction, *Nature* **458**, 178 (2009).
- [55] X. Y. Lü, Y. Wu, J. R. Johansson, H. Jing, J. Zhang, and F. Nori, Squeezed Optomechanics with Phase-Matched Amplification and Dissipation, *Phys. Rev. Lett.* **114**, 093602(2015).